

NACA RM L54A27

NACA

TECH LIBRARY KAFB, NM
0144322

RESEARCH MEMORANDUM

ZERO-LIFT DRAG OF SEVERAL CONICAL AND BLUNT NOSE
SHAPES OBTAINED IN FREE FLIGHT AT MACH
NUMBERS OF 0.7 TO 1.3

By Robert O. Piland and Leonard W. Putland

Langley Aeronautical Laboratory
Langley Field, Va.

NATIONAL ADVISORY COMMITTEE
FOR AERONAUTICS

WASHINGTON
March 23, 1954

Classification cancelled (or changed to Unclassified)

By Authority of NASA TTPs Amendment #121
(OFFICER AUTHORIZED TO CHANGE)

By 4 Nov. 57.....
NAME AND

..... NK.....
GRADE OF OFFICER MAKING CHANGE)

..... 30 Mar. 61.....
DATE



0144322

NACA RM L54A27

~~CONFIDENTIAL~~

NATIONAL ADVISORY COMMITTEE FOR AERONAUTICS

RESEARCH MEMORANDUM

ZERO-LIFT DRAG OF SEVERAL CONICAL AND BLUNT NOSE
SHAPES OBTAINED IN FREE FLIGHT AT MACH
NUMBERS OF 0.7 TO 1.3

By Robert O. Piland and Leonard W. Putland

SUMMARY

The zero-lift drag characteristics of seven nose shapes on a slender body of revolution have been determined in free flight between Mach numbers of 0.7 and 1.3 corresponding to Reynolds numbers, based on body length, of 6×10^6 and 11×10^6 , respectively. The nose shapes tested consisted of a spherical segment, a flat face with a sharp shoulder, a flat face with a rounded shoulder, 30° and 40° total-angle cones, and a spherical segment with each of two different-length spikes projecting upstream from the center of the nose.

The flat nose with the rounded shoulder was found to have considerably less subsonic drag than the flat nose with the sharp shoulder. This beneficial effect deteriorates at transonic speeds and disappears at supersonic speeds. Both flat noses have considerably higher drag than the spherical segment at supersonic speeds. The 30° and 40° conical noses were found to have somewhat lower drag than the spherical segment at a Mach number of 1.3 but the differences are small. Adding a spike to the spherical segment had no appreciable effect for the Mach number range tested.

INTRODUCTION

Conventional slender nose shapes have been found undesirable for use with certain proposed missiles due to the optical requirements of the guidance systems. Consequently, effort has been directed toward the study of the aerodynamic characteristics of blunt nose shapes (refs. 1 to 6). During these studies, improvement of blunt-nose characteristics has been attempted by modifications to the nose. These modifications have most often taken the form of spikes protruding upstream from the center of the nose. Investigations, except those in free flight (refs. 1 and 5), have been conducted at Mach numbers above 1.6. Since missiles

~~CONFIDENTIAL~~*Handwritten:* H-54-1527

which might use blunt shapes, with or without modifications, will operate through a range of Mach numbers, the drag characteristics of these shapes are of interest at lower speeds for the purpose of performance estimation.

In addition to their use for missiles, blunt shapes are being considered in the design of bombs, in order to avoid difficulties in launching from high-speed aircraft and in an attempt to reduce dispersion.

With these points in mind, the Langley Pilotless Aircraft Research Division has tested a limited number of nose shapes in the Mach number range of 0.7 to 1.3 to supplement the aforementioned higher speed data. Drag data have been obtained for seven nose shapes on a fin-stabilized body of revolution in free flight. Reynolds numbers of the tests, based on body length, were 6×10^6 to 11×10^6 corresponding to Mach numbers from 0.7 to 1.3. The tests were conducted at the Langley Pilotless Aircraft Research Station, Wallops Island, Va. using the helium gun.

MODELS AND TESTS

The seven nose shapes tested are shown in figure 1 and are numbered 1 to 7. Nose shape 1 is shown on the test body. All other nose shapes except 3 were also tested on this body. The test body for nose shape 3 is shown in the figure also. This nose shape has the same diameter, flat face, as model 2, but the test body was modified between stations 1.53 and 4.50 as can be seen in the figure. Model ordinates are presented in table I.

The models were constructed of mahogany with 24S-T aluminum-alloy bases. Three equally spaced fins, located as shown in figure 1, stabilized the models in flight. All models were finished smoothly with clear lacquer. Photographs of the models are shown in figure 2, with the exception of model 3 for which no photograph is available. The models were fired from a helium gun (ref. 7) and attained a peak Mach number of 1.3. During the coasting period that followed, a continuous velocity record was obtained by means of a CW Doppler radar. Atmospheric conditions were obtained by means of a radiosonde. A trajectory was calculated from the velocity-time record which in turn gave the variation of altitude and flight-path angle with time. Deceleration of the model was determined by differentiation of the velocity-time curve. With this information, used in conjunction with atmospheric data, the drag coefficient of the model may be calculated as follows:

$$C_D = - \frac{W}{qSg} (a + g \sin \gamma)$$

w weight of model, lb
g acceleration due to gravity, 32 ft/sec²
S maximum frontal area, sq ft
q dynamic pressure, $\frac{1}{2}\rho V^2$, lb/sq ft
a acceleration, ft/sec²
 γ flight-path angle, deg

The accuracy of the tests is believed to be within the following limits:

C_D ± 0.01
M ± 0.01

Test conditions as indicated by the variation of Reynolds number with Mach number are presented in figure 3. Reynolds numbers are based on body length.

RESULTS AND DISCUSSION

Drag coefficients for models 1, 2, and 3, based on maximum frontal area, are presented in figure 4 for Mach numbers from 0.7 to 1.26. As expected, model 1 has the lowest drag of all three models. Removing the spherical segment (model 2) results in a large increase in drag which can be associated in part with a separated region on the forward part of the nose. A spark photograph in reference 8 shows this separated region very graphically. Modifying the nose shape of model 2 by the rounding of a shoulder (model 3) is seen to have considerable effect. This rounded shoulder was obtained by modifying the forebody aft of the flat face while retaining the same-diameter flat face on model 3 as on model 2. At lower subsonic speeds model 3 has the same drag as model 1, indicating elimination of the separated region. At transonic speeds, the beneficial effects of the rounded shoulder decrease and, above a Mach number of 1.13, the pressure drag on the rounded shoulder itself causes the drag of model 3 to be even greater than that of model 2. As mentioned above, the diameters of the flat faces of models 2 and 3 were the same. This diameter was kept constant so that the two models could house the same-size seeker lens. If, in a particular case, it is not necessary to keep the diameter constant, both subsonic and supersonic benefits may be effected by rounding the shoulder and reducing the amount of flat area. The forebody radii will then decrease for several stations aft of the flat face.

Since the subsonic benefits of the shoulder are so large, data from another investigation, partially reported in reference 1, are shown in figure 5. The very similar results for these shapes on a different test body tend to confirm the present findings. As mentioned in the introduction, consideration is being given to the use of bomb shapes with flat noses. These data indicate that with a minimum of modification the drag of a flat nose could be reduced considerably at subsonic speeds. Emphasis is placed here on the bomb rather than the missile since this speed range is probably of more importance to bomb designers than missile designers.

Figure 6 presents the drag coefficients for the spherical segment (model 1) and the 30° (model 4) and 40° (model 5) conical-nose models. The coefficients at Mach number 1.25 are in the expected order. Model 4 seems to be reaching its peak drag at a lower Mach number than model 5. This is consistent with the relative Mach numbers for shock attachment on the two cones.

The drag coefficients for models 1, 6, and 7 are presented in figure 7. References 2, 3, and 4 have shown substantial reductions in drag to be effected by the addition of a spike ahead of a spherical segment for Mach numbers as low as 1.6. The present tests, however, indicate the spike to have a negligible effect at Mach numbers of 1.3 or lower. Reference 3 also shows a decreasing beneficial effect with decreasing Mach number. In addition, reference 3 shows that, for an optimum spike length, the drag was about the same as that of a 42° total-angle cone for the Mach number range tested (1.76 to 2.10). If this holds true at the lower Mach numbers, large benefits could not be expected from the spike since the drag of the conical nose of 42° angle is not greatly lower than that of the spherical segment alone. This can be seen by referring to figure 6 where the drag of the 40° conical-nose model is compared with that of the model with the spherical-segment nose.

CONCLUDING REMARKS

Seven nose shapes have been tested in free flight on a fin-stabilized body, and drag data have been obtained between Mach numbers of 0.7 and 1.3, corresponding to Reynolds numbers of 6×10^6 and 11×10^6 , based on body length. The nose shapes are a spherical segment, a flat face with a sharp shoulder, a flat face of similar area with a rounded shoulder, 30° and 40° total-angle cones, and a spherical segment with each of two different-length spikes. The following observations were made from the tests:

1. The large subsonic and transonic drag penalty occasioned by the removal of a spherical segment, leaving a flat face, may be greatly reduced by rounding the sharp shoulder.

2. At a Mach number of 1.2, 30°, and 40° conical nose shapes have only slightly less drag than the spherical-segment nose shape.

3. Spikes protruding upstream from a spherical-segment nose have negligible beneficial effect for the Mach number range tested.

Langley Aeronautical Laboratory,
National Advisory Committee for Aeronautics,
Langley Field, Va., January 12, 1954.

REFERENCES

1. Wallskog, Harvey A., and Hart, Roger G.: Investigation of the Drag of Blunt-Nosed Bodies of Revolution in Free Flight at Mach Numbers From 0.6 to 2.3. NACA RM L53D14a, 1953.
2. Jones, Jim J.: Flow Separation From Rods Ahead of Blunt Noses at Mach Number 2.72. NACA RM L52E05a, 1952.
3. Moeckel, W. E.: Flow Separation Ahead of a Blunt Axially Symmetric Body at Mach Numbers 1.76 to 2.10. NACA RM E51I25, 1951.
4. Beastall, D., and Turner, J.: The Effect of a Spike Protruding in Front of a Bluff Body at Supersonic Speeds. TN No. Aero. 2137, British R.A.E., Jan. 1952.
5. Piland, Robert O.: Preliminary Free-Flight Investigation of the Zero-Lift Drag Penalties of Several Missile Nose Shapes for Infrared Seeking Devices. NACA RM L52F23, 1952.
6. Gapcynski, John P., and Robins, A. Warner: The Effect of Nose Radius and Shape on the Aerodynamic Characteristics of a Fuselage and a Wing-Fuselage Combination at Angles of Attack. NACA RM L53I23a, 1953.
7. Hall, James Rudyard: Comparison of Free-Flight Measurements of the Zero-Lift Drag Rise of Six Airplane Configurations and Their Equivalent Bodies of Revolution at Transonic Speeds. NACA RM L53J21a, 1953.
8. Richards, E.: Comparative Dispersion and Drag of Spheres and Right Cylinders. Rep. No. 717, Ballistic Res. Labs., Aberdeen Proving Ground, 1950.

TABLE I.- BODY ORDINATES OF MODELS AFT OF STATION 1.53

[Dimensions are in inches]

Models 1, 2, and 4 to 7

Station	Radius
1.530	0.300
1.722	.324
2.095	.363
2.469	.391
4.157	.494
4.500	.500
13.00	.500
15.00	.360

Model 3

Station	Radius
1.530	0.300
1.824	.420
4.157	.494
4.500	.500
13.00	.500
15.00	.360

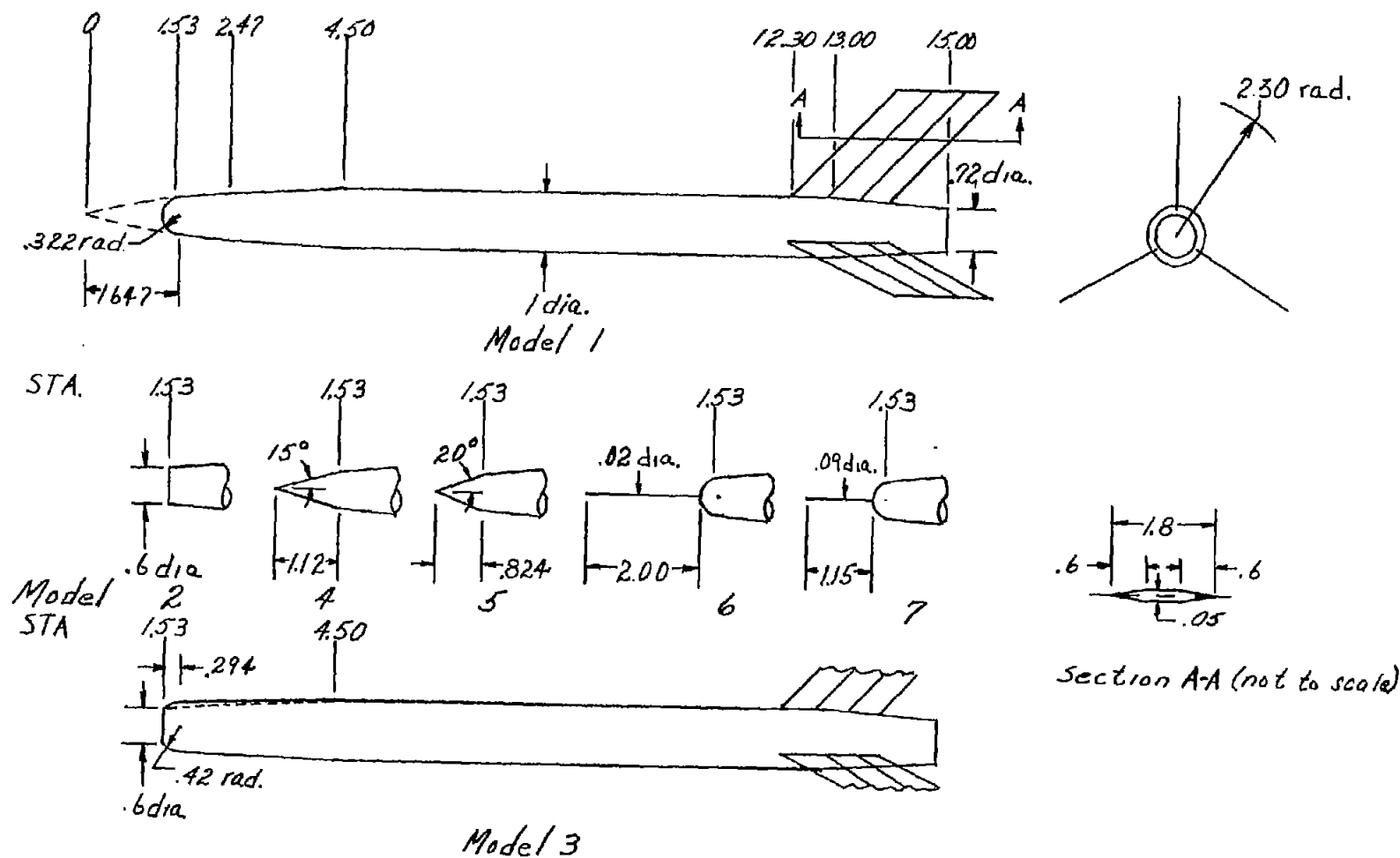
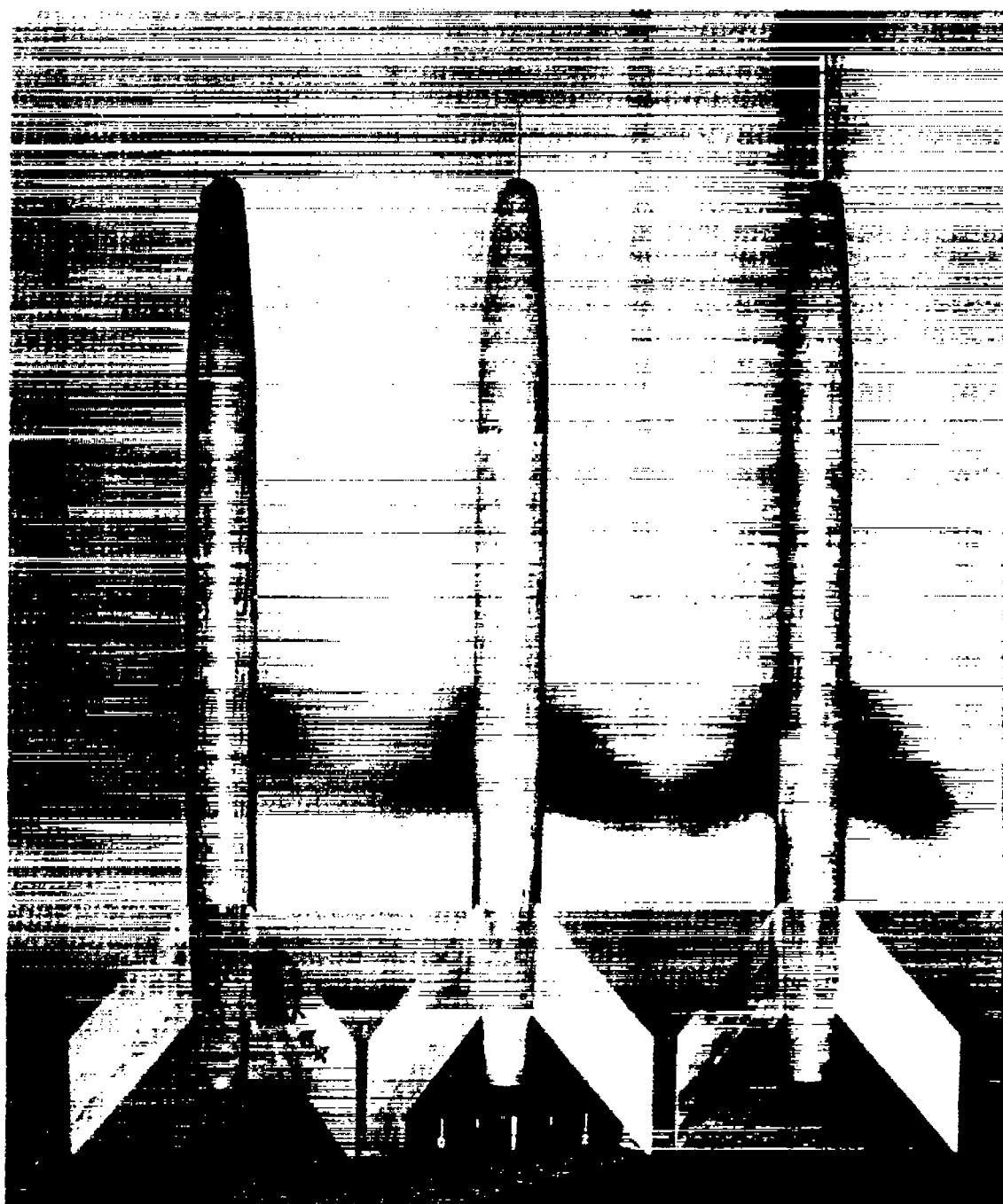


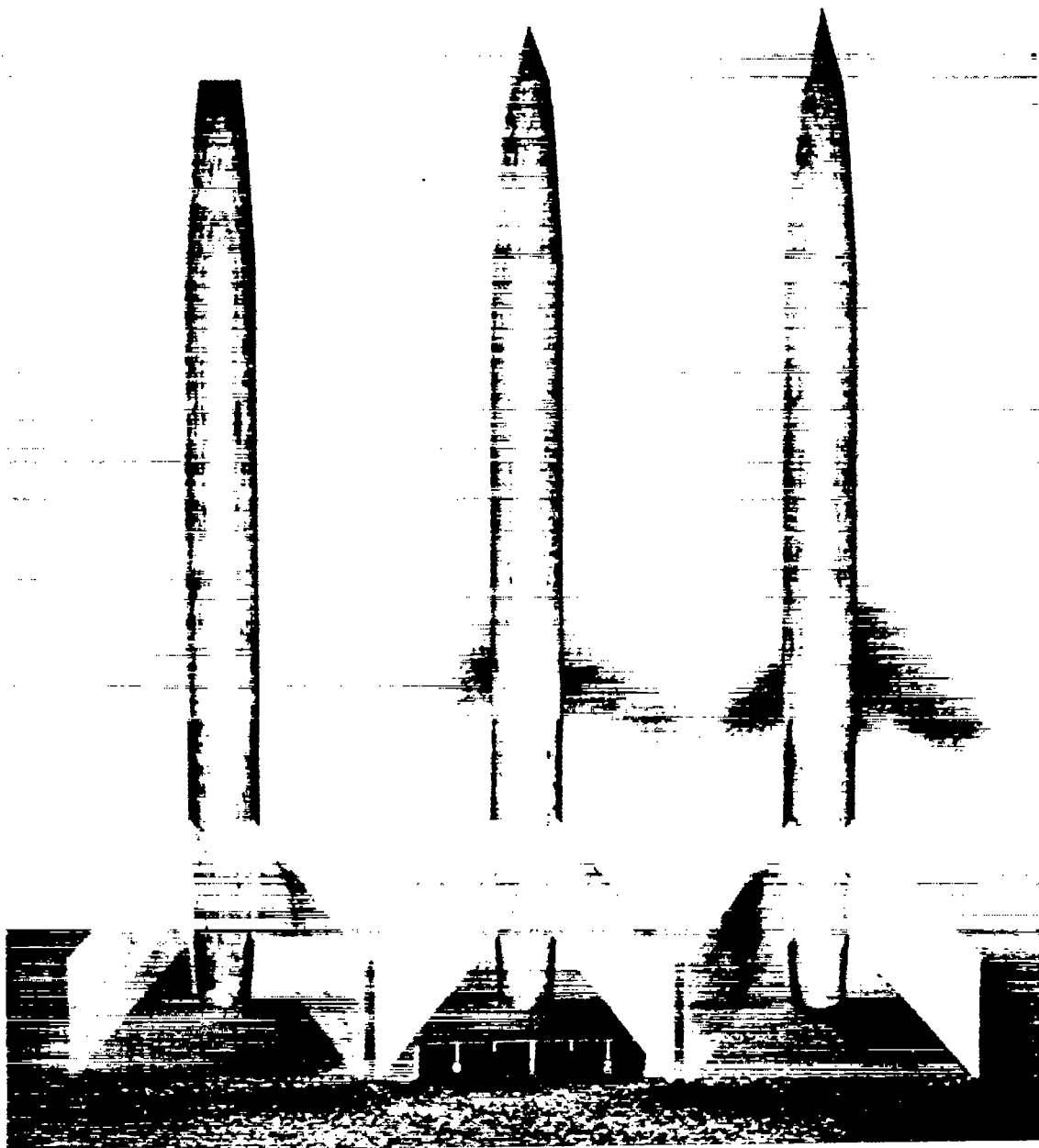
Figure 1.- Sketch of models tested.



(a) Models 1, 6, and 7.

L-80396

Figure 2.- Photographs of models.



(b) Models 2, 4, and 5.

L-80397

Figure 2.- Concluded.

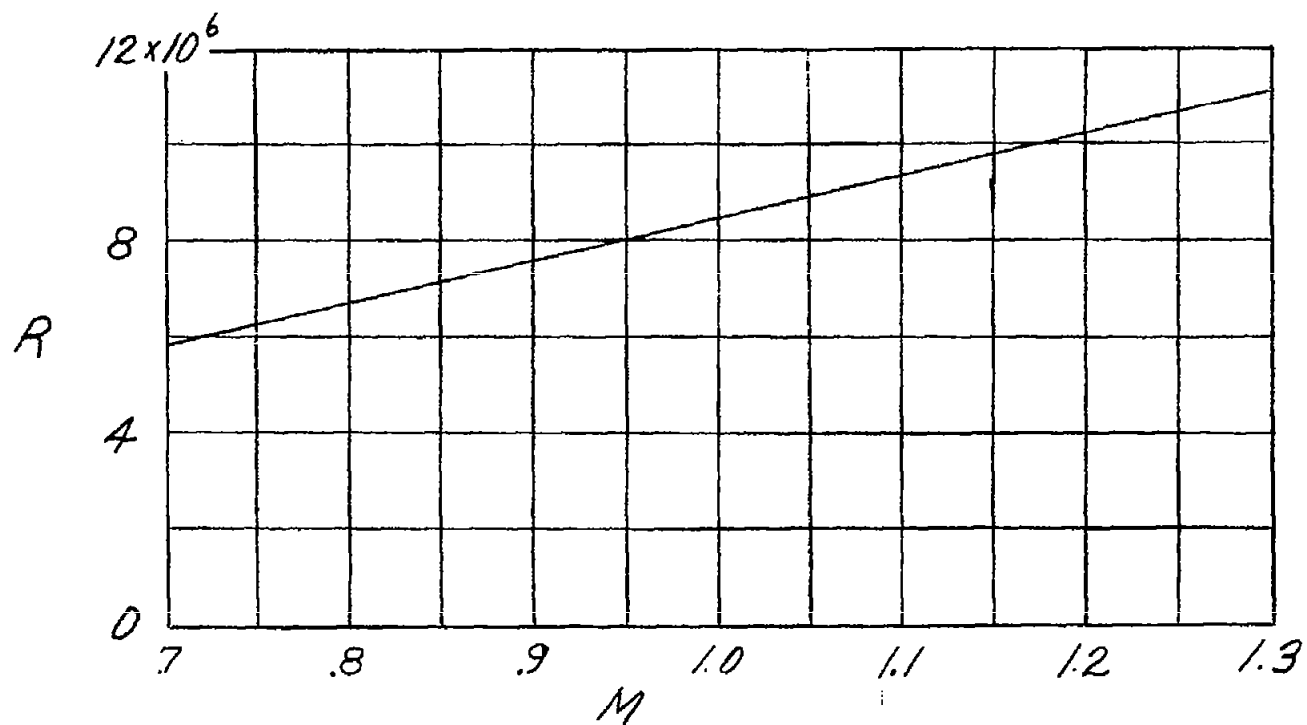


Figure 3.- Test Reynolds numbers based on body length.

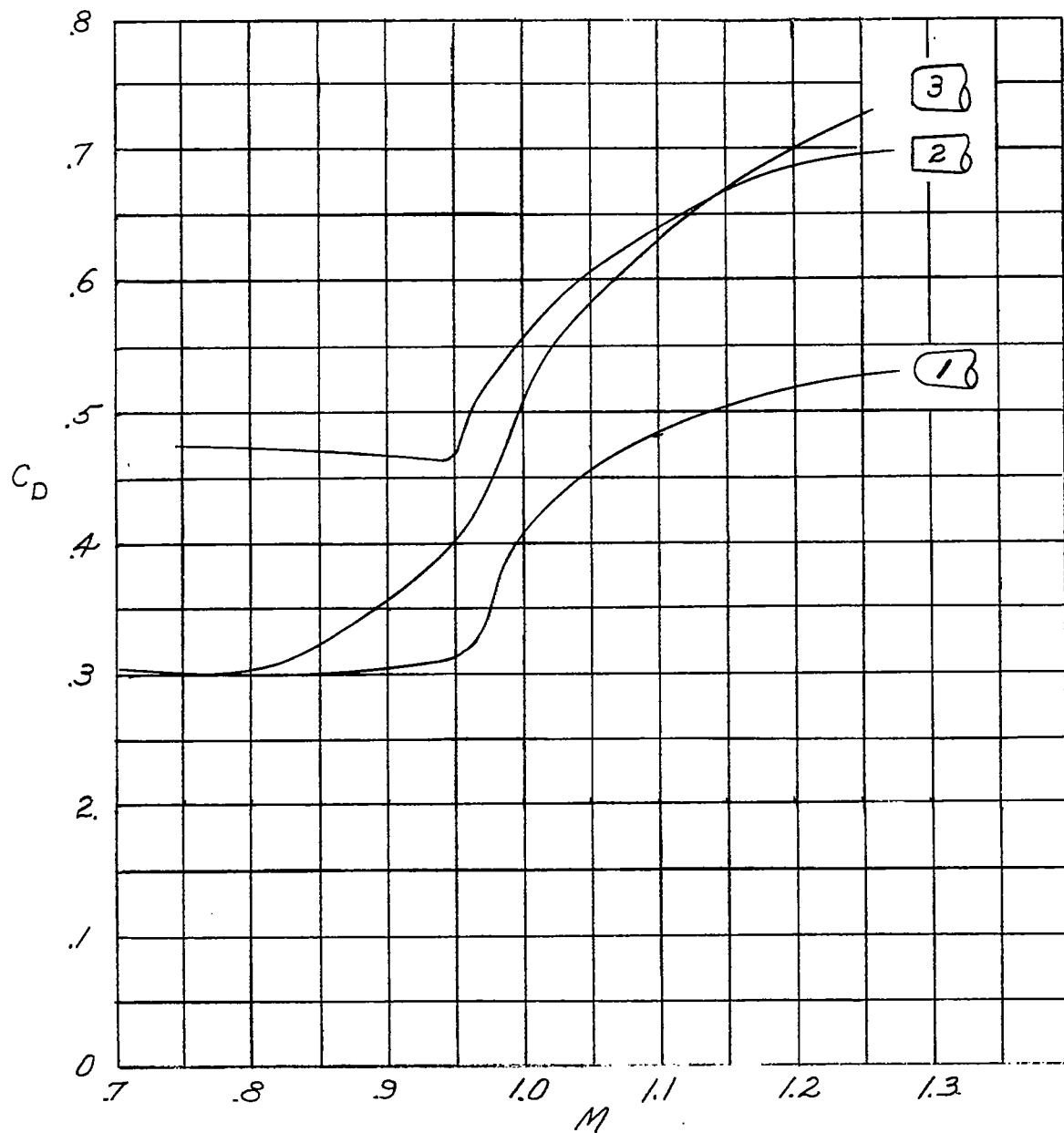


Figure 4.- Drag coefficients of models 1, 2, and 3.

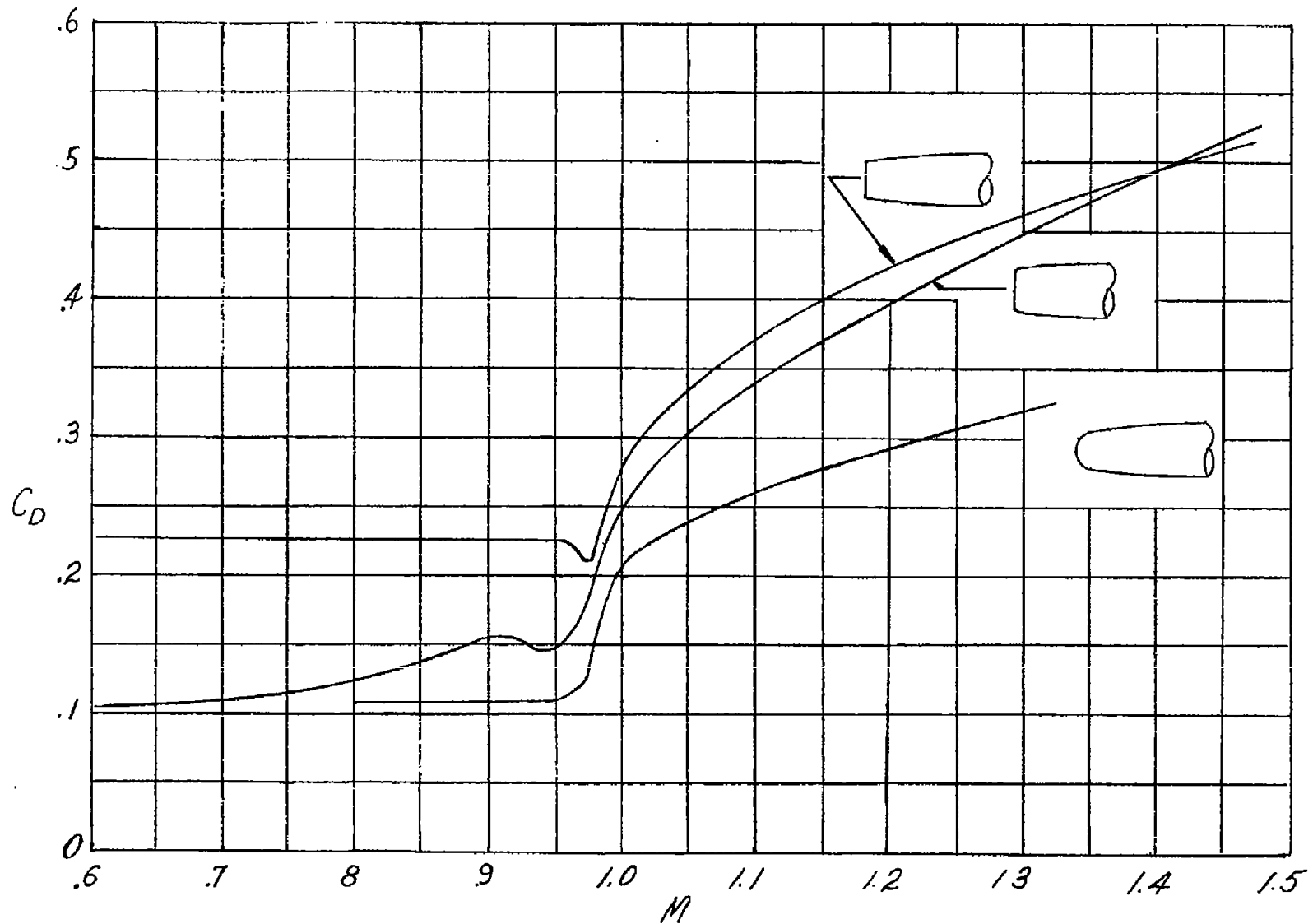


Figure 5.- Drag coefficients for three models with nose shapes similar to those of models 1, 2, and 3. Data from reference 1.

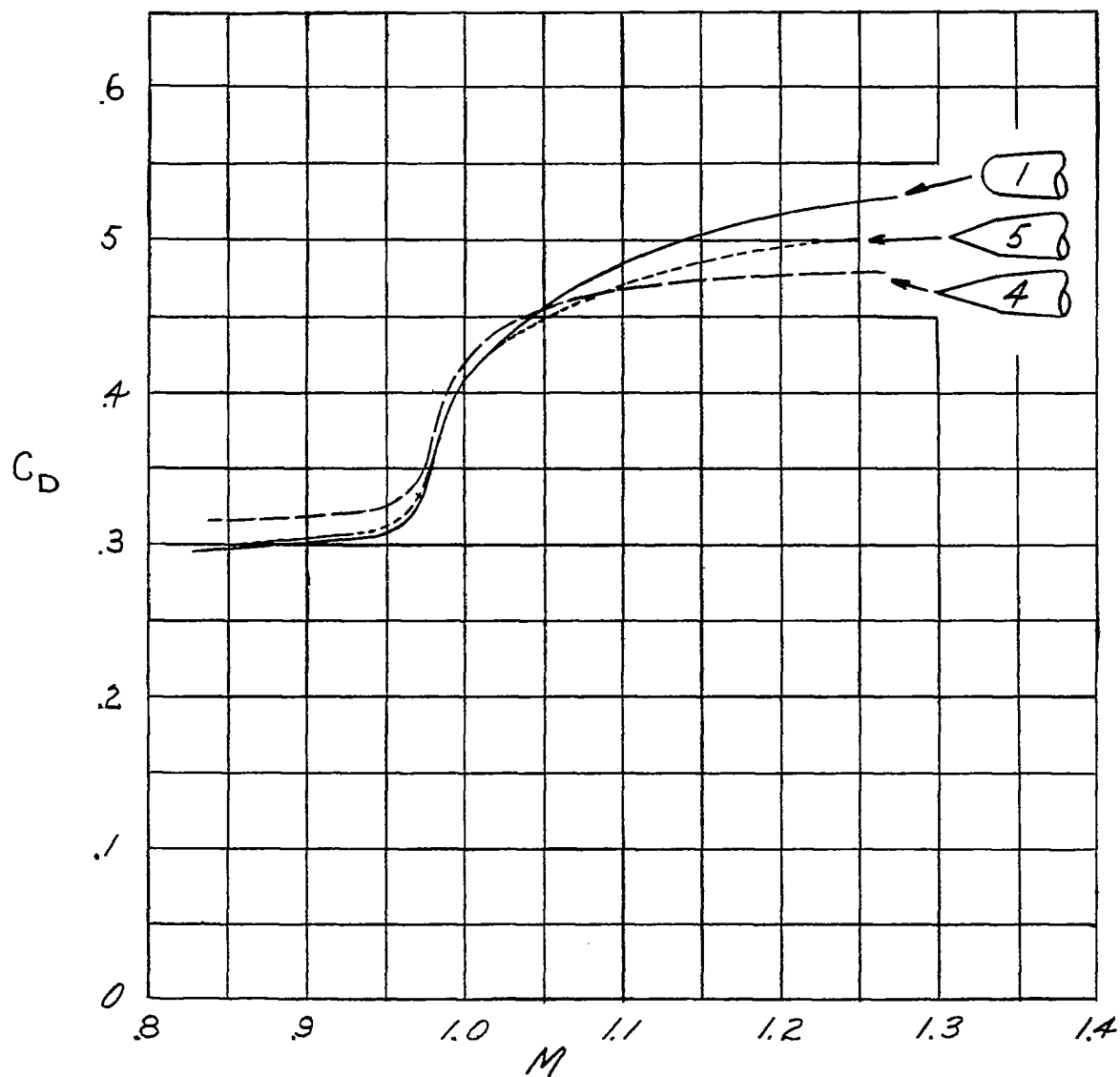


Figure 6.- Drag coefficients for models 1, 4, and 5.

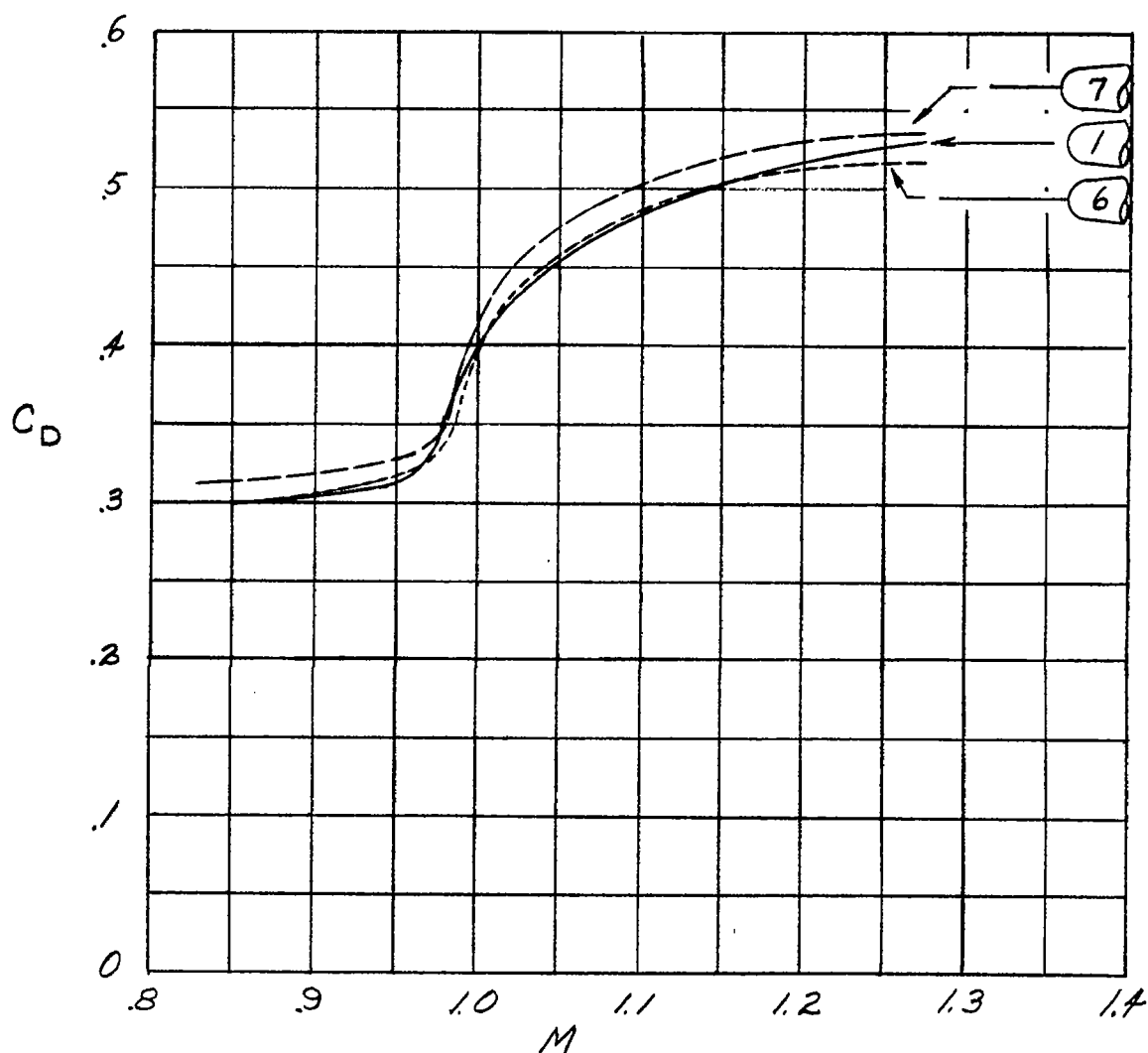


Figure 7.- Drag coefficients for models 1, 6, and 7.